A Unified Continuous Staging Framework for Alzheimer's Disease and Lewy Body Dementia via Hierarchical Anatomical Features

Tong Chen[1], Minheng Chen[1], Jing Zhang[1], Yan Zhuang[1], Chao Cao[1], Xiaowei Yu[1], Yanjun Lyu[1], Lu Zhang[2], Li Su[3,4], Tianming Liu[5], and Dajiang Zhu[1(✉)]

[1] Department of Computer Science and Engineering, University of Texas at Arlington, USA
{dajiang.zhu@uta.edu}
[2] Department of Computer Science, Indiana University Indianapolis, USA
[3] Sheffield Institute for Translational Neuroscience, University of Sheffield, UK
[4] Department of Psychiatry, University of Cambridge, UK
[5] School of Computing, University of Georgia, USA

Abstract. Alzheimer's Disease (AD) and Lewy Body Dementia (LBD) often exhibit overlapping pathologies, leading to common symptoms that make diagnosis challenging and protracted in clinical settings. While many studies achieve promising accuracy in identifying AD and LBD at earlier stages, they often focus on discrete classification rather than capturing the gradual nature of disease progression. Since dementia develops progressively, understanding the continuous trajectory of dementia is crucial, as it allows us to uncover hidden patterns in cognitive decline and provides critical insights into the underlying mechanisms of disease progression. To address this gap, we propose a novel multi-scale learning framework that leverages hierarchical anatomical features to model the continuous relationships across various neurodegenerative conditions, including Mild Cognitive Impairment, AD, and LBD. Our approach employs the proposed hierarchical graph embedding fusion technique, integrating anatomical features, cortical folding patterns, and structural connectivity at multiple scales. This integration captures both fine-grained and coarse anatomical details, enabling the identification of subtle patterns that enhance differentiation between dementia types. Additionally, our framework projects each subject onto continuous tree structures, providing intuitive visualizations of disease trajectories and offering a more interpretable way to track cognitive decline. To validate our approach, we conduct extensive experiments on our in-house dataset of 308 subjects spanning multiple groups. Our results demonstrate that the proposed tree-based model effectively represents dementia progression, achieves promising performance in intricate classification task of AD and LBD, and highlights discriminative brain regions that contribute to the differentiation between dementia types. Our code is available at https://github.com/tongchen2010/haff.

Keywords: Alzheimer's Disease · Lewy Body Dementia · Dementia Progression · Cortical folding pattern · Multi-scale fusion · 3-Hinge Gyrus

1 Introduction

Alzheimer's Disease (AD) and Lewy Body Dementia (LBD) are two of the most common neurodegenerative disorders, with AD accounting for 60–80% of cases and LBD contributing approximately 4.2% [1,18]. Both lead to irreversible brain changes, severe cognitive decline, and ultimately death. Early diagnosis and studying disease progression are crucial, as they enable patients and families to plan care. [1]. However, differentiating AD and LBD is challenging due to overlapping neuropathological and symptomatic features. For example, LBD patients may also exhibit beta-amyloid plaques typical of AD, while AD patients can show parkinsonian symptoms resembling Parkinson Disease Dementia, a subtype of LBD [8]. This overlap often results in misdiagnosis and delayed diagnosis, approximately 18 months for LBD and 14.8 months for young AD patients after initial hospital visit [10]. Although current AD biomarkers—such as CSF Aβ 42/Aβ40 ratios, tau tests, and plasma ptau181—are effective, they are invasive, expensive, and not widely accessible, prompting interest in non-invasive alternatives like structural magnetic resonance imaging (sMRI) and diffusion tensor imaging (DTI) for differential diagnosis [19,24].

Recent advancements in deep learning have demonstrated promising performance in the early diagnosis of AD[22,21]. However, many of these approaches are primarily focused on classification tasks, which limits their ability to capture the continuous progression of dementia. A recent study introduced a tree embedding framework that models the continuous progression of AD by encoding anatomical features across different disease stages [23]. This framework not only achieves state-of-the-art performance in multi-class classification but also projects patient data onto a tree-like structure, facilitating a more intuitive visualization of AD progression. Despite these strengths, the approach relies on coarse anatomical features, potentially overlooking small brain regions that are critical for distinguishing between overlapping dementia syndromes. For instance, previous research has noted that only limited areas within the temporal lobe exhibit significantly greater cortical thinning in AD compared to LBD [13,28,29], therefore, it's necessary to include fine-scale measures to differentiate AD and LBD. Furthermore, its application is limited to AD and does not demonstrate the capacity to address the complexities of multi-dementia progression.

To overcome the limitations of prior work, we propose a multi-scale feature fusion framework that captures hierarchical anatomical characteristics to model the continuous transitions of various dementia stages, CN, MCI, AD and LBD. Our method employs a graph neural network-based model to integrate structural connectivity (SC) and cortical folding pattern features at different scales so that it captures the fine-grained regional differences that's able to differentiate AD and LBD. Coarse regions are derived from the neuroanatomical atlas, ensuring consistency with well-established cortical parcellation framework. In contrast, hub-based patches are obtained using an innovative cortical folding pattern representation, namely 3-Hinge Gyrus (3HG) [2,3,26] where 3HG is defined by the conjunction of gyri from three different directions. 3HG can serve as cor-

tical hubs [27] and 3HG connectomes has outperforms traditional region-based connectomes in classifying AD stages, underscoring the benefits of finer-scale brain region [11]. The Multi-scale Graph Embedding Fusion (MGEF) block of our method effectively combines the graph emebddings of both atlas-based and hub-based anatomical features, enabling improved differentiation between AD and LBD. To validate our approach, we conducted extensive experiments on our in-house dataset, demonstrating its effectiveness in addressing the intricate task of differentiating four brain conditions and visualizing the dementia progression.

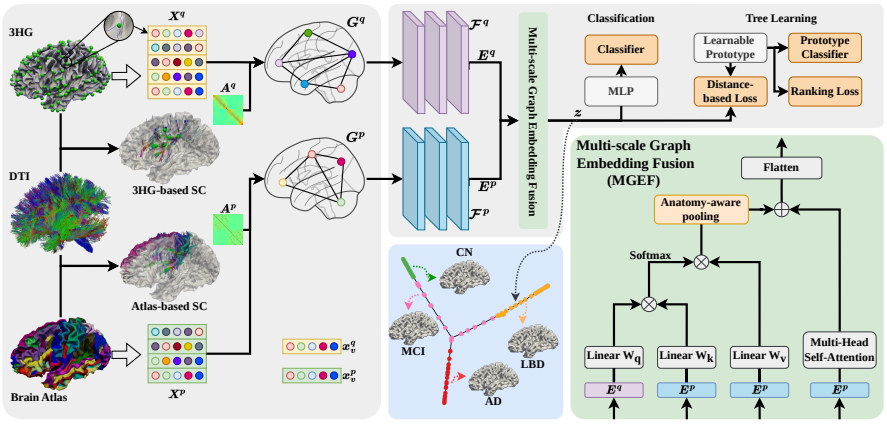

Fig. 1. illustrates our overall framework. For each subject, we generate two graphs: one for atlas-based and one for 3HG-based anatomical features. We feed the graph data into our proposed framework, which learns meaningful representations for classification and subsequently generates a tree structure to visualize dementia progression.

2 Methods

2.1 Anatomical Feature Selection

We leverage vertex-based cortical features (CF) to characterize cortical morphology, including cortical thickness (CTh), curvature, sulcal depth (SD), local gyrification index (LGI), and fractal dimension (FD). CTh, SD, curvature, and LGI are derived using Freesurfer tools [5], while FD is computed with our in-house tool using the Minkowski–Bouligand dimension. Notably, measures such as CTh have been shown to correlate strongly with dementia severity and are widely used to differentiate clinical stages such as AD, CN, and MCI [12,20]. Additionally, FD quantifies the complexity of cortical patterns by examining changes across different scales, and has recently emerged as a valuable metric for assessing cortical atrophy in dementia [17,30].

2.2 Modal Architecture

Graph Convolution Network Fig. 1 illustrates the overview of our proposed framework. Each subject is characterized by two types of graph inputs, namely $G^p = (\mathcal{V}^p, \mathcal{E}^p)$ for atlas-based data and $G^q = (\mathcal{V}^q, \mathcal{E}^q)$ for 3HG-based data, where $\mathcal{V}$ denotes a set of nodes and $\mathcal{E}$ denotes a set of edges connecting those nodes. For any node v, its feature is denoted by x_v and the matrix X represents the features of all nodes. The edge between nodes u and v is denoted by e_{vu}, and the adjacency matrix A is constructed from these edges, representing the SC. The label for each subject is given by y. For the model, we first employ two dual graph convolutional networks (GCN) [9], defined by functions $\mathcal{F}(\cdot)$ that operate on the respective graph data. The node embeddings for the two modalities are computed as $E^p = \mathcal{F}^p(X^p, A^p)$ and $E^q = \mathcal{F}^q(X^q, A^q)$, where $E^p \in \mathbb{R}^{r\times k}$ and $E^q \in \mathbb{R}^{s\times k}$ denote the node embeddings for each graph input projected into a k-dimensional latent space, with r and s being the numbers of atlas regions and 3HG, respectively.

Multi-scale Anatomy-aware Fusion After $\mathcal{F}(\cdot)$, E^p are fed into a multi-head self-attention block to capture the global contextual information of X^p. In contrast, instead of applying self-attention to X^q, we introduce a cross attention mechanism, termed *Anatomy-aware Cross Attention*(ACA)(Eq. 1), that enables each x_v^q, identified by its label m_v to query the corresponding X^p. This mechanism allows the 3HG nodes to extract relevant information from the atlas regions. The cross attention is formulated as follows:

$$\begin{aligned} Q^q = E^q W_Q, \quad K^p = E^p W_K, \quad V^p = E^p W_V, \\ \text{Attention}(Q^q, K^p, V^p) = \text{softmax}\left(\frac{Q^q {K^p}^\top}{\sqrt{d_k}}\right) V^p, \end{aligned} \tag{1}$$

where W_Q, W_K, and W_V are learnable projection matrices, and d_k is the dimensionality of the node embeddings. Following the cross-attention mechanism, we perform our proposed *Anatomy-aware Mean Pooling*(AMP)(Eq. 2). In the equation, R_j represents a set of x^q located in atlas region j and $e_i^q \in \mathbb{R}^d$ is the embedding of node x_i^q. AMP aggregates the x^q in each atlas region, and if a region has no 3HG (i.e., $|R_j| = 0$), its pooled embedding is defined as the zero vector in $\mathbb{R}^d$.

$$m_j = \begin{cases} \dfrac{1}{|R_j|} \displaystyle\sum_{i\in R_j} e_i^q, & \text{if } |R_j| > 0, \\ \mathbf{0} \in \mathbb{R}^d, & \text{if } |R_j| = 0. \end{cases} \tag{2}$$

Finally, the pooled 3HG embeddings are combined with the atlas region embeddings by a simple element-wise sum to form the final feature representation $Z = E^p + E^q$, which is then processed for classification using cross-entropy loss and tree structure learning.

2.3 Tree Structure Learning

Prototype Model Firstly a set of a learnable prototype embeddings are defined as $\mathscr{E}_{\text{learn}} = \{e_i \in \mathbb{R}^k \mid i = 1, 2, \ldots, C\}$, where $\mathscr{E}_{\text{learn}}$ represents the learnable parameters for C classes in the k-dimensional latent space where $k = r \times d$. Each prototype embedding e_i represents a class y_i in the latent space. Then we minimize the distance between the z_i and its corresponding prototype embeddings e_i using l2 distance and the distance-based loss of each sample towards its corresponding prototype center is formulated as $\mathcal{L}_{\text{distance}} = \|z_i - e_y\|_2^2$ where e_y is the corresponding class embedding of the input x_i. To enhance generalization, a batch-wise mean squared error (MSE) loss over b samples was incorporated into the overall loss function: $\mathcal{L}_{\text{MSE}} = \frac{1}{b}\sum_{i=1}^{b} \|h(x_b, \theta) - e_y\|^2$. The tree loss combines the distance loss and MSE loss where α is a hyperparameter:

$$\mathcal{L}_{\text{tree}} = \mathcal{L}_{\text{distance}} + \alpha \mathcal{L}_{\text{MSE}} \tag{3}$$

Learnable Prototype Embedding A set prototype embeddings $\mathcal{E}_{\text{init}} \in \mathbb{R}^{C \times k}$ is firstly initialized such that all prototype embeddings are equally spaced in terms of euclidean distance. The learnable embedding matrix $\mathcal{E}_{\text{learn}} \in \mathbb{R}^{C \times k}$ is defined by $\mathcal{E}_{\text{learn}} = \mathcal{E}_{\text{init}} \cdot W + b$ where W and b are learnable parameters. Prototype learning consists of two loss functions:
a. Classification loss ensures the learnable prototype embeddings are aligned with their class labels using a cross-entropy loss. $\mathcal{L}_{\text{classification}}$ is the classification loss of the prototype embedding to its corresponding label.
b. Ranking Loss [4] is adopted as a regularization term and also to capture the prior knowledge of known orders between classes (e.g., CN $\rightarrow$ MCI $\rightarrow$ AD). The similarity-based adjacency matrix S is constructed based on the following:

$$S_{i,j} = \begin{cases} s_0 & \text{if } \text{label}_i = \text{label}_j, \\ s_p & \text{if } |\text{label}_i - \text{label}_j| = d_p, \quad \text{for } p = 1, 2, \ldots, k, \\ 0 & \text{otherwise.} \end{cases} \tag{4}$$

Here, i and j denote the row and column indices of the matrix. The term s_0 represents the self-similarity values when labels are identical. The values $s_1, s_2, \ldots, s_k$ are predefined similarity values corresponding to neighboring classes at increasing distances. The thresholds $d_1, d_2, \ldots, d_k$ define specific distances between labels that establish adjacency, where each d_p corresponds to similarity level s_p. This setup ensures that similarity values are applied based on both label proximity and predefined distance thresholds. To normalize the adjacency matrix, we compute the Laplacian matrix $\mathbb{L}_y = S - D_s$, where D_s is the degree matrix of S. Using this Laplacian matrix, the order constraint loss is defined as:

$$\mathcal{L}_{\text{ranking}} = \text{trace}(O_{\text{logit}} \cdot \mathbb{L}_y \cdot O_{\text{logit}}^T) \tag{5}$$

The final loss for prototype embedding learning combines the classification loss and the order constraint loss where β is a hyperparameter(Eq. 5) as follows:

$$\mathcal{L}_{\text{prototype}} = \mathcal{L}_{\text{classification}} + \beta \mathcal{L}_{\text{ranking}} \tag{6}$$

3 Experiments

3.1 Dataset

Data Preprocessing. In our study, we analyzed a dataset comprising T1-weighted sMRI and DTI scans from 308 subjects, including 77 cognitively normal (CN), 77 MCI, 77 AD, and 77 LBD subjects. All T1-weighted MRI scans underwent standardized preprocessing procedures as described in [25]. In brief, the preprocessing included brain extraction using the FMRIB Software Library (FSL), cortical surface reconstruction for both white matter and pial surfaces, and subsequent parcellation based on the Destrieux Atlas using the FreeSurfer toolkit [5]. DTI data were similarly preprocessed with fiber tracking conducted using DSI Studio.

3.2 Implementation Details

All experiments were conducted using 5-fold cross-validation. The GCN model was implemented with two GCN layers, and each multi-head attention block consisted of four attention heads. For training, all models were run with 100 epochs with a batch size of 16 and a dropout rate of 0.3. Regarding optimization, we employed the AdamW optimizer together with the ReduceLROnPlateau scheduler. Specific hyperparameters included a learning rate of 0.001 for the classification model and $\alpha = 0.1$ and $\beta = 0.3$ for the prototype model.

4 Results

Table 1. Comparison of classification performance metrics for distinguishing among CN, MCI, AD, and LBD using various methods and feature combinations.

Method	Groups	Feature	Accuracy (%)	Sensitivity (%)	Specificity (%)	F1 (%)
Nemoto *et al.* [16]	AD vs LBD	VB	79.15 ± 5.22	81.54 ± 10.43	76.77	N/A
Nakatsuka *et al.* [15]	AD vs LBD	VB	75.00	80.00	64.00	N/A
Goto *et al.* [7]	AD vs LBD	VB	70.00	N/A	N/A	N/A
MLP	CN vs MCI vs AD vs LBD	SC	57.10 ± 6.19	57.10 ± 5.95	85.7 ± 2.03	56.79 ± 5.56
SVM	CN vs MCI vs AD vs LBD	SC	55.79 ± 8.14	55.79 ± 8.14	85.26 ± 2.69	55.46 ± 8.02
Random Forest	CN vs MCI vs AD vs LBD	SC	54.85 ± 5.02	54.85 ± 5.02	84.94 ± 1.65	54.07 ± 5.15
Logistic Regression	CN vs MCI vs AD vs LBD	SC	55.48 ± 7.94	55.54 ± 7.85	85.17 ± 2.63	54.76 ± 7.65
Our method	CN vs MCI vs AD vs LBD	CF+SC	**61.68 ± 3.12**	**61.35 ± 4.80**	**87.19 ± 1.07**	**57.42 ± 5.76**

4.1 Classification

Table 1 summarizes the classification performance for CN, MCI, AD, and LBD. Because of the pathological and symptomatic overlap, differentiating AD from LBD is particularly challenging. Previous studies have primarily focused on

simpler binary comparisons, such as AD versus LBD using voxel-based (VB) method [7,15,16], rather than tackling the complexity of a four-class classification task. Traditional classifiers using only SC achieved moderate accuracies between 54.85% and 57.42%, reflecting the inherent difficulty of the problem. In contrast, our innovative approach, which seamlessly integrates CF with SC, achieved a notable accuracy of 61.68%, demonstrating the effectiveness of multimodal feature integration.

4.2 Top discriminative atlas region and 3HG

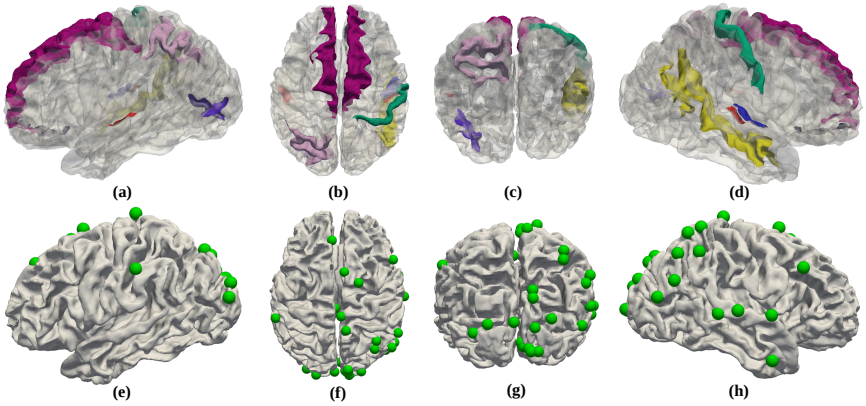

Fig. 2. (a)–(d) present the 10 most discriminative atlas regions, while (e)–(h) showcase the top 30 discriminative 3HG features for classification.

Fig. 2 shows the top 10 Destrieux regions contributing to the classification task. In particular, Fig. 2(b) and (d) highlight the superior frontal gyri in both hemispheres, consistent with studies linking impairments in working memory and attention to AD [14]. Additionally, Fig. 2(d) underscores the superior temporal sulcus (STS), with prior work reporting an approximate 50% loss in AD, which may relate to social and cognitive deficits [6]. Fig. 2(c) draws attention to occipital regions, potentially linked to visual hallucinations in LBD. Fig. 2(e)–(h) present the top 30 discriminative 3HG features for classification. This approach allows for the detection of microstructural changes that may be missed by traditional atlas-based methods. By complementing the atlas-based analysis, the 3HG features enhance the sensitivity of the classification task, potentially leading to improved diagnostic accuracy.

4.3 Embedding Tree

For the tree structure generation, we adopted a distance-based method proposed in [23]. In Fig. 3, we present 10 learned trees to demonstrate the stability of the

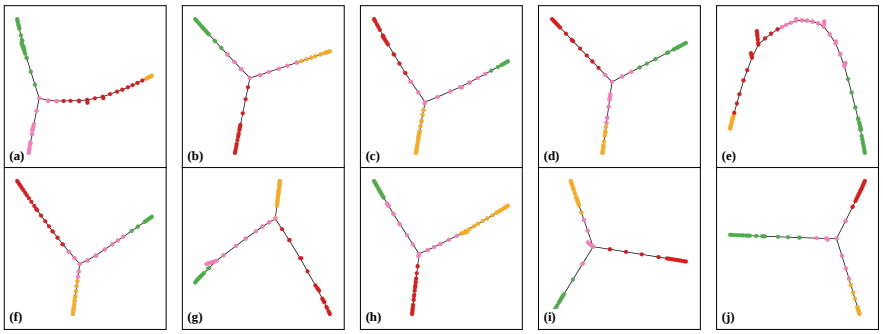

Fig. 3. Each panel (a-j) presents a disease embedding tree learned by the proposed framework, showing how individual subjects (represented by circles) cluster according to their disease stage. The four disease stages are color-coded: CN in **green**, MCI in pink, AD in **red**, and LBD in orange.

tree structures. Although each tree's structure shows some variability, they consistently reveal a key pattern: LBD subjects tend to cluster in close proximity to MCI and AD subjects. This clustering on the tree structure suggests that the anatomical and connectivity features captured by our model reflect underlying similarities in the disease progression of LBD relative to MCI and AD. Fig. 3(b-d),(f-j) predominantly indicate that LBD subjects are positioned near MCI subjects while panels Fig. 3(a) and (e) show LBD subjects clustering closer to AD subjects. The tree structures provide a continuous representation of patient status. By observing patients onto the disease tree, we can learn their brain state within the cohort. These tree structures offer a continuous representation of patient status, allowing us to map each patient's brain state within the cohort. By situating patients on the disease tree, we can compare their progression relative to others and gain insights into the continuum of dementia progression.

5 Conclusion

In this study, we introduce a novel multi-scale learning framework that captures hierarchical anatomical features and effectively models continuous relationships across various dementia conditions. Our approach not only outperforms both traditional and deep learning models in a multi-dementia classification task but also provides a comparative and interpretable visualization of patient progression through a tree-structured representation. This tree structure offers valuable insights into disease trajectories, enabling a more nuanced understanding of neurodegenerative progression. Furthermore, our framework identifies the most discriminative atlas regions and 3HG features, highlighting key regions that distinguish different forms of dementia.

Acknowledgments. This study was supported by the National Institutes of Health (R01AG075582 and RF1NS128534) and funded by the Sir Jules Thorn Charitable

Trust (05/JTA), Wellcome Trust Intermediate Clinical Fellowship (WT088441MA), Alzheimer's Research UK Senior Research Fellowship (ARUK-SRF2017B-1), The Lewy body Society (LBS/002/2019) and NIHR Biomedical Research Centres in Sheffield, Cambridge and Newcastle. We also thank Andrew M. Blamire, John-Paul Taylor, Li Su and John T. O'Brien for sharing the data.

Disclosure of Interests. The authors have no competing interests to declare that are relevant to the content of this article.

References

1. 2024 alzheimer's disease facts and figures. Alzheimer's & Dementia **20**(5), 3708–3821 (2024)
2. Chen, H., Li, Y., Ge, F., Li, G., Shen, D., Liu, T.: Gyral net: A new representation of cortical folding organization. Medical Image Analysis **42**, 14–25 (2017)
3. Chen, M., Cao, C., Chen, T., Zhuang, Y., Zhang, J., Lyu, Y., Yu, X., Zhang, L., Liu, T., Zhu, D.: Using structural similarity and kolmogorov-arnold networks for anatomical embedding of cortical folding patterns. In: 2025 IEEE 22nd International Symposium on Biomedical Imaging (ISBI). pp. 1–5. IEEE (2025)
4. Chen, W., Liu, T.y., Lan, Y., Ma, Z.m., Li, H.: Ranking measures and loss functions in learning to rank. In: Bengio, Y., Schuurmans, D., Lafferty, J., Williams, C., Culotta, A. (eds.) Advances in Neural Information Processing Systems. vol. 22. Curran Associates, Inc. (2009)
5. Fischl, B.: Freesurfer. NeuroImage **62**(2), 774–781 (2012)
6. Gómez-Isla, T., Hollister, R., West, H., Mui, S., Growdon, J.H., Petersen, R.C., Parisi, J.E., Hyman, B.T.: Neuronal loss correlates with but exceeds neurofibrillary tangles in alzheimer's disease. Annals of Neurology: Official Journal of the American Neurological Association and the Child Neurology Society **41**(1), 17–24 (1997)
7. Goto, H., Ishii, K., Uemura, T., Miyamoto, N., Yoshikawa, T., Shimada, K., Ohkawa, S.: Differential diagnosis of dementia with lewy bodies and alzheimer disease using combined mr imaging and brain perfusion single-photon emission tomography. American Journal of Neuroradiology **31**(4), 720–725 (2010)
8. Gurnani, A.S., Gavett, B.E.: The differential effects of alzheimer's disease and lewy body pathology on cognitive performance: a meta-analysis. Neuropsychology Review **27**(1), 1–17 (Mar 2017)
9. Kipf, T.N., Welling, M.: Semi-Supervised Classification with Graph Convolutional Networks. In: Proceedings of the 5th International Conference on Learning Representations. ICLR '17 (2017)
10. Kvello-Alme, M., Bråthen, G., White, L.R., Sando, S.B., Knopman, D.: Time to diagnosis in young onset alzheimer's disease: A population-based study from central norway. Journal of Alzheimer's Disease **82**(3), 965–974 (2021)
11. Lyu, Y., Zhang, L., Yu, X., Cao, C., Liu, T., Zhu, D.: Mild cognitive impairment classification using a novel finer-scale brain connectome. In: 2024 IEEE International Symposium on Biomedical Imaging (ISBI). pp. 1–5 (2024)
12. Mak, E., Su, L., Williams, G.B., Watson, R., Firbank, M., Blamire, A.M., O'Brien, J.T.: Longitudinal assessment of global and regional atrophy rates in alzheimer's disease and dementia with lewy bodies. NeuroImage: Clinical **7**, 456–462 (2015)

13. Mak, E., Su, L., Williams, G.B., Watson, R., Firbank, M.J., Blamire, A.M., O'Brien, J.T.: Progressive cortical thinning and subcortical atrophy in dementia with lewy bodies and alzheimer's disease. Neurobiology of Aging **36**(4), 1743–1750 (2015)
14. Miller, E.K., Cohen, J.D.: An integrative theory of prefrontal cortex function. Annual review of neuroscience **24**(1), 167–202 (2001)
15. Nakatsuka, T., Imabayashi, E., Matsuda, H., Sakakibara, R., Inaoka, T., Terada, H.: Discrimination of dementia with lewy bodies from alzheimer's disease using voxel-based morphometry of white matter by statistical parametric mapping 8 plus diffeomorphic anatomic registration through exponentiated lie algebra. Neuroradiology **55**(5), 559–566 (May 2013)
16. Nemoto, K., Sakaguchi, H., Kasai, W., Hotta, M., Kamei, R., Noguchi, T., Minamimoto, R., Arai, T., Asada, T.: Differentiating dementia with lewy bodies and alzheimer's disease by deep learning to structural mri. Journal of Neuroimaging **31**(3), 579–587 (2021)
17. Núñez, C., Callén, A., Lombardini, F., Compta, Y., Stephan-Otto, C., for the Alzheimer's Disease Neuroimaging Initiative: Different cortical gyrification patterns in alzheimer's disease and impact on memory performance. Annals of Neurology **88**(1), 67–80 (2020)
18. Vann Jones, S.A., O'Brien, J.T.: The prevalence and incidence of dementia with lewy bodies: a systematic review of population and clinical studies. Psychological Medicine **44**(4), 673–683 (2014)
19. Wang, L., Thompson, P.M., Zhu, D.: Analyzing mild cognitive impairment progression via multi-view structural learning. In: Chung, A.C.S., Gee, J.C., Yushkevich, P.A., Bao, S. (eds.) Information Processing in Medical Imaging. pp. 656–668. Springer International Publishing, Cham (2019)
20. Wee, C.Y., Yap, P.T., Shen, D., for the Alzheimer's Disease Neuroimaging Initiative: Prediction of alzheimer's disease and mild cognitive impairment using cortical morphological patterns. Human Brain Mapping **34**(12), 3411–3425 (2013)
21. Zhang, J., Lyu, Y., Yu, X., Zhang, L., Cao, C., Chen, T., Chen, M., Zhuang, Y., Liu, T., Zhu, D.: Classification of mild cognitive impairment based on dynamic functional connectivity using spatio-temporal transformer. arXiv preprint arXiv:2501.16409 (2025)
22. Zhang, J., Yu, X., Lyu, Y., Zhang, L., Chen, T., Cao, C., Zhuang, Y., Chen, M., Liu, T., Zhu, D.: Brain-adapter: Enhancing neurological disorder analysis with adapter-tuning multimodal large language models. arXiv preprint arXiv:2501.16282 (2025)
23. Zhang, L., Wang, L., Liu, T., Zhu, D.: Disease2vec: Encoding alzheimer's progression via disease embedding tree. Pharmacological Research **199**, 107038 (2024)
24. Zhang, L., Wang, L., Zhu, D.: Recovering brain structural connectivity from functional connectivity via multi-gcn based generative adversarial network. In: Medical Image Computing and Computer Assisted Intervention–MICCAI 2020: 23rd International Conference, Lima, Peru, October 4–8, 2020, Proceedings, Part VII 23. pp. 53–61. Springer (2020)
25. Zhang, L., Wang, L., Zhu, D.: Predicting brain structural network using functional connectivity. Medical Image Analysis **79**, 102463 (2022)
26. Zhang, L., Zhao, L., Liu, D., Wu, Z., Wang, X., Liu, T., Zhu, D.: Cortex2vector: anatomical embedding of cortical folding patterns. Cerebral Cortex **33**(10), 5851–5862 (12 2022)
27. Zhang, T., Li, X., Jiang, X., Ge, F., Zhang, S., Zhao, L., Liu, H., Huang, Y., Wang, X., Yang, J., Guo, L., Hu, X., Liu, T.: Cortical 3-hinges could serve as

hubs in cortico-cortical connective network. Brain Imaging and Behavior **14**(6), 2512–2529 (Dec 2020)
28. Zhu, D., Li, K., Guo, L., Jiang, X., Zhang, T., Zhang, D., Chen, H., Deng, F., Faraco, C., Jin, C., et al.: Dicccol: dense individualized and common connectivity-based cortical landmarks. Cerebral cortex **23**(4), 786–800 (2013)
29. Zhu, D., Li, K., Terry, D.P., Puente, A.N., Wang, L., Shen, D., Miller, L.S., Liu, T.: Connectome-scale assessments of structural and functional connectivity in mci. Human brain mapping **35**(7), 2911–2923 (2014)
30. Ziukelis, E.T., Mak, E., Dounavi, M.E., Su, L., T O'Brien, J.: Fractal dimension of the brain in neurodegenerative disease and dementia: A systematic review. Ageing Research Reviews **79**, 101651 (2022)